www.sciencemag.org/content/355/6320/68/suppl/DC1

Supplementary Materials for

Microstructural proliferation in human cortex is coupled with the development of face processing

Jesse Gomez, Michael A. Barnett, Vaidehi Natu, Aviv Mezer, Nicola Palomero-Gallagher, Kevin S. Weiner, Katrin Amunts, Karl Zilles, Kalanit Grill-Spector*

*Corresponding author. Email: kalanit@stanford.edu

Published 6 January 2017, *Science* **355**, 68 (2017)
DOI: 10.1126/science.aag0311

This PDF file includes:

Materials and Methods
Figs. S1 to S10
Table S1
References

Materials and Methods

Participants

26 neurologically typical children ages 5-12 years (mean age 8.5 ± 2.2 years, 12 females) and 26 adults ages 22-28 years old (mean age 24 ± 1.6 years, 9 females) participated in these experiments. Age ranges were chosen in children to *(i)* maximize a wide dynamic range of functional and structural development reported previously (*2, 3, 21, 22*), and *(ii)* maximize the success of MRI measurements without having to discard a substantial number of participants due to excessive motion in the scanner, which is a common issue with pediatric neuroimaging (*23*). Because our goal was to link structural changes with functional and behavioral ones, we couldn't focus on younger age groups where acquiring such data is unfeasible. A similar range of ages was chosen in adults when most structural and functional development in VTC is thought to be near completion (*15, 24*). Following data quality thresholds discussed below, 4 children and 1 adult were excluded from further analysis (22 children, 25 adults remain). Participants had normal or corrected-to-normal vision and were screened to have no prior or current psychiatric conditions. All procedures were approved to be in accordance with the Institutional Review Board of Stanford University. Prior to the experiment, adult participants and parents provided written informed consent, and children provided written assent.

Each subject participated in several sessions to distribute the various scans and assessments to avoid fatigue. Each of the following sessions was thus performed on a different day; all sessions were completed over the period of a few months. *(i)* Participants under the age of 18 completed training in a mock scanner employing live feedback of head motion during the viewing of a 15-minute movie. This acclimated the participants to the scanner environment and reduced motion. Participants were advanced to functional and anatomical scanning if they could lie still (less than 2.4 mm of head motion) for the duration of mock scanning. Participants complete the place recognition memory task on this day. *(ii)* All participants participated in an MRI session in which we obtained anatomical MRI and qMRI measurements. *(iii)* All participants participated in an fMRI session in which we measured brain responses to stimuli of various categories. *(iv)* After completion of all MRI scans, and on a separate day, participants participated in the behavioral experiment testing face recognition ability outside the scanner (in addition to other experiments related to other projects). Importantly, qMRI quantifies absolute tissue values, rather than relative intensities, and is indicative of the underlying tissue

microarchitecture (*25*), facilitating direct comparisons of the cortical tissue volume and make-up across individuals (*4, 5, 26*).

To ensure high quality data we measured motion during functional MRI, as this is the largest source of noise in pediatric imaging (*23*). We excluded participants who moved more than 2 voxels based on criteria used in prior pediatric imaging studies (*3, 22*). 4 children and 1 adult were excluded from data analysis based on excessive head motion during fMRI or head-motion artifacts visible in qMRI. Remaining participants had less than 2 voxels of motion, with no significant difference between children (1.08 mm ± 0.53 mm) and adults (0.88 mm ± 0.48 mm). Thus, results presented in the manuscript reflect data from 22 children and 25 adults. Additionally, the number of participants in which each functional region of interest (fROI) could be defined and the number of participants who completed a given behavioral test are presented in Table S1 below. Likewise, the number of participants present in a given figure is described in the figure legend.

Table S1: The number of participants per fROI and number of participants with behavioral data.

	pFus		CoS		mFus		pOTS		mOTS		CMFT	Place
	left	right	left	right	left	right	left	right	left	right		recognition
Children	20	20	21	20	16	16	13	15	13	N/A	21	22
Adults	19	20	25	22	21	21	25	24	23	N/A	22	22

Data acquisition

Quantitative magnetic resonance imaging (qMRI): Data were collected on a 3-Tesla GE Discovery MR750 scanner (GE Medical Systems) at the Center for Cognitive Neurobiological Imaging at Stanford University using a phase-array 32-channel head coil. Quantitative MRI measurements are obtained from the protocols set forth in (*4*). T_1 relaxation times were measured from four spoiled gradient echo (spoiled-GE) images with flip angles of 4°, 10°, 20°, 30° (TR=14 ms, TE=2.4 ms) and a scan resolution of 0.8x0.8x1.0 mm^3 (later resampled to 1mm isotropic). For the purposes of removing field inhomogeneities, we collected four additional spin echo inversion recovery (SEIR) scans with an echo planar imaging (EPI) read-out, a slab inversion pulse, and spectral spatial fat suppression. The SEIRs were acquired with a TR of 3 s,

echo time set to minimum full, and 2x acceleration. The inversion times were 50, 400, 1200, and 2400 ms, and were collected at a 2x2 mm^2 in-plane resolution and a slice thickness of 4 mm.

Functional MRI: Data were collected on hardware described above. Functional data were collected with a simultaneous multi-slice EPI sequence with a multiplexing factor of 3 (*27*) to acquire near whole-brain (48 slices) volumes at TR=1s, TE=30ms; flip angle = 76^o; FOV = 192mm. Data were acquired at a resolution of 2.4mm isotropic voxels with one-shot T2*-sensitive gradient echo sequence with slices aligned parallel to the parieto-occipital sulcus.

fMRI category localizer experiment: During scanning, participants viewed stimuli from 5 categories each containing two subcategories (Faces: child, adult; Bodies: whole, limbs; Places: corridors, houses; Objects: cars, guitars; Characters: pseudowords, numbers). Images from each subcategory were presented in 4 s mini-blocks at a rate of 2 Hz as described previously (*28*) intermixed with 4s blank mini-blocks; presentation order of trial types was counterbalanced. Each run was 5 min, 24 s long, and each subject completed 3 runs. Participants were instructed to fixate on a central point, and perform an oddball task, detecting a randomly-presented phase scrambled image within a block.

Data Analysis

QMRI data analysis: Both the spoiled-GE and the SEIR scans were processed using the mrQ software package in MATLAB to produce the T_1 and MTV maps. The mrQ analysis pipeline corrects for RF coil bias using SEIR-EPI scans, producing accurate proton density (PD) and T_1 fits across the brain. Using individual participants' voxels containing CSF within the ventricles, maps of macromolecular tissue volume (MTV) are produced calculating the fraction of a voxel that is non-water (CSF voxels are taken to be nearly 100% water). The full analysis pipeline and its published description can be found at (https://github.com/mezera/mrQ)(*26*). Images of all individual subject's $\mathbf{T_1}$ maps across ventral temporal cortex (VTC) are shown in Fig. S9.

fMRI data analysis: Data were processed and analyzed in MATLAB using mrVista software (http://github.com/vistalab) as in previous publications (*28*). Functional data were

aligned to an artificial T_1-weighted volume optimized for tissue segmentation through FreeSurfer produced from the qMRI scans to ensure accurate alignment between functional and quantitative volumes. Alignment of functional data was validated for each subject by comparing mean maps of BOLD data to each subject's brain anatomy (Fig. S10). Functional data were unsmoothed and always analyzed within each individual subject's brain space. Functional data were restricted to the cortical ribbon using hand-fixed cortical segmentations produced from FreeSurfer. This same cortical mask was later applied to qMRI volumes to avoid sampling voxels within white matter or dura.

Functional data were motion corrected both within and between scans. Any participants who moved more than 2 voxels within a scan were either excluded from data analysis or invited back for another session, such that children and adults were matched for data quality (i.e. no differences in motion). Each voxel's data was (1) transformed from arbitrary scanner units to percentage signal by dividing each time point by the average response across the entire experiment and (2) was fit with a general linear model (GLM) by convolving the stimulus presentation design with the hemodynamic function (HRF) implemented in SPM (www.fil.ion.ucl.ac.uk/spm). We also used the GLM to generate statistical maps of contrasts between different conditions.

Definition of functional regions of interest (fROIs, see Fig. 1 and Fig. S8): Statistical contrasts of faces (places or characters) vs. all other stimuli were thresholded at t-values > 3, voxel-level, in each subject. Spatially contiguous clusters of face-selective voxels that responded more strongly to faces than other stimuli and were located in the posterior lateral fusiform gyrus were defined as pFus-faces (also referred to as fusiform face area one, FFA-1(*29*)). More anterior face-selective voxels near or overlapping the anterior tip of the mid fusiform sulcus (MFS) were defined as mFus-faces (also referred to as fusiform face area two, FFA-2). Together, pFus-faces and mFus-faces are also referred to as the fusiform face area (FFA)(*29*). Place-selective cortex was defined as a cluster of voxels responding significantly more to places than other stimuli in the collateral sulcus (CoS-places) also referred to as the parahippocampal place area (PPA)(*30*). Word-selective regions for supplemental analyses were defined as cluster of voxels significantly selective for characters (pseudowords, numbers) over all other stimuli. These clusters were located in the posterior occipitotemporal sulcus bilaterally (pOTS-chars, also referred to as visual

word form area one, VWFA1) and a cluster in the middle OTS (mOTS-chars, also referred to as VWFA2)(*28, 31, 32*). MOTS-chars could only be reliably localized in the left hemisphere. Because we were not able to identify all fROIs in every subject, each fROI data contains the subset of participants in which we were able to identify that fROI; the number of participants in each analysis is listed in Table S1, the manuscript, and corresponding figures.

Estimating functional selectivity using a leave-one-run-out analysis (LORO): In order to assess functional selectivity of a given fROI in an unbiased way, we used a LORO analysis. Here we used a subset of the functional data (2 runs) to define the fROI based on the contrast of interest and then measured the selectivity on the left-out run of the functional data. Selectivity is measured as the mean t-value across voxels from the left-out run, for the contrast of interest (e.g. faces > non faces). This analysis was done for all combinations of left-out runs and averaged across all 3 iterations. To ensure that our data was in the same anatomical location across permutations, we constrained the face-selective fROI to be within the lateral fusiform gyrus and the place-selective fROI to be in the collateral sulcus by dilating the original fROIs defined from all three runs to create an anatomical mask. From the same fROI we used to estimate selectivity in the left-out run on each iteration, we measured the qMRI values; we report the average value across the three iterations for the correlation analysis in Fig. 2. This provided a measure of T_1 relaxation time and MTV from the same fROI from which functional selectivity was calculated.

We also repeated the LORO analysis in fROIs that were matched in size across children and adults. Because smaller fROIs in children could potentially produce noisier or biased measures of functional selectivity and T_1, we increased the size of children's fROIs to the mean size of adult participants' fROIs, which is on average a 30% increase. At the step of the LORO analysis in which t>3 voxels produced from 2 runs of data were acquired, the number of voxels was increased by 30% by randomly sampling (using 100 bootstrap iterations) from voxels neighboring the t>3 voxels within the anatomically dilated ROI. By bootstrapping and averaging, we fairly sample the cortex surrounding the central peak of selectivity without any spatial bias towards those voxels immediately surrounding the center, as a simple dilation approach might do.

Behavioral measurements

All participants completed place recognition testing before scanning, and face recognition testing after all scanning sessions had been completed. 22 adults and 21 children completed face and place recognition tests (see Table S1). We chose these behavioral tasks for the following reasons: *(i)* Face recognition ability has been shown to have a protracted developmental process compared to other tasks (*33-35*), allowing us to observe cortical development in the presence or absence of behavioral development. *(ii)* Prior developmental research shows a relationship between the size of face- and place-selective cortex with face and place recognition memory, respectively. *(iii)* Having more than one task allows us to test if there is a nonspecific behavioral development, or a category-specific development.

Face recognition memory was assessed using a version of the Cambridge Face Memory Test (CFMT) presenting child faces instead of adult faces (*36*). This avoids floor behavioral performance observed in children when testing their performance in the original CFMT, which uses adult male faces. In this self-paced test, participants learn the identity of six target faces. In the test phase consisting of 72 trials, participants are required to identify the learned faces amongst distractors, as described in the original version (*37*). As the test progresses the judgments are made more difficult as faces appear in novel views, lighting, and with superimposed noise. Accuracy was measured as the percent correct responses made during the test phase. Data are shown in Fig. 2.

Place recognition memory was assessed using an old-new recognition task developed in our lab employing scenes of indoor corridors and outdoor buildings (in addition to other stimuli including words, faces, cars, and limbs). After an initial viewing phase in which participants perform a one-back task, indicating when two consecutive images are identical, and then a three-minute intervening phase in which participants fixated on a rotating checkerboard wedge, participants saw original stimuli from the viewing phase in addition to distractor stimuli in a recognition phase. Participants reported for each stimulus whether it was ‘old’ or ‘new’, with 16 ‘old’ and 16 ‘new’ exemplars of each category. Participants were not informed that there would be a memory test following the viewing of visual stimuli to control for possible differences in rehearsal mechanisms between participants of different ages. While not identical, the two recognition tasks are similarly organized in that they require participants to view initial face or place stimuli, and then distinguish these stimuli from distractors of the same category at a later

time. Percent correct scores on the face and place recognition tests were correlated against selectivity and T_1 of a given fROI (Fig. 2B). Three adults and one child were unable to complete the behavioral assay and were not included in these correlations.

Children showed no significant differences in performance between the face and place recognition tests ($t(41) = 0.65$, n.s.). Adults performed significantly better at face recognition than place recognition ($t(42) = 9.25$, $p<0.001$), which is perhaps to be expected if face but not place recognition improves with development.

Statistical Analyses

To test for development of T_1 across ventral temporal cortex (VTC), we conducted an analysis of variance (ANOVA) on T_1 using as factors age group (adult/child), fROI (pFus-faces/CoS-places), and hemisphere (right/left).

When comparing across age groups within an ROI or comparing within an age group across we use two tailed t-tests. All tests were considered significant if they passed a Bonferroni-corrected threshold. We used a Bonferroni corrected threshold of 0.05/8 comparisons (4 fROIs (pFus/mFus/Cos/pOTS) and 2 hemispheres (left/right)) < 0.00625.

In all correlation analyses each data point was a subject. Correlations that were found to be significant (beyond Bonferroni correction) were subjected to second analysis in which we used a stepwise multivariate linear model in which the dependent variable was fit using a linear model with two independent factors- the factor of interest and age. This procedure 'partials out age' because we can test if the factor of interest contributes significantly to the observation in addition to age. We then report which correlations were significant after partialling our age

Simulations of myelin development in cortex

Modeling the increase in nerve fiber diameter across development (Fig. 3E): We sought to model the required radial increase of myelin that could account for the increase in MTV in face-selective cortex between childhood and adulthood. Myelin, due to its rich macromolecule and lipid content (cholesterol, sphingomyelin, etc.), has a complex relation to T_1 that is difficult to model. However, myelin volume linearly contributes to MTV (the fraction of a voxel's volume belonging to non-water), as progressive increases in myelin volume proportionally increase MTV (*4*).

We first estimated the distribution of MTV values in each group, and calculated the difference in means across these distributions. This reveals a 12.6% increase in the mean distribution of MTV values from childhood to adulthood.

Using the difference of cylindrical volumes, illustrated to the right and expressed in equation 1, we calculate R_2 (the final end radius of the nerve fiber after simulated myelination) given the observed difference in tissue volume fraction as a function of R_1 (starting nerve fiber radius of the model) and number of fibers in a voxel (N_A, see equation 2).

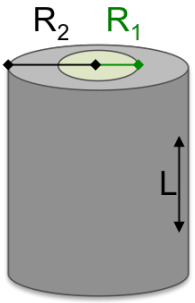

$$1 \quad N_A\left[(\pi R_2^2 L) - (\pi R_1^2 L)\right] = \Delta V$$

$$2 \quad R_2 = \sqrt{\frac{\Delta V}{N_A \pi L} + (R_1)^2}$$

In the simulation we tested a range of possible parameters values for N_A and R_1 and use the following constants for axon length (L) and volume change (ΔV). ***L:*** the mean length of an axon, assuming even distribution of neurons within a voxel, is 0.5mm. The average change in macromolecular tissue volume (ΔV) was estimated based on our observed 12.6% increase in MTV, which is 7.8×10^7 μm^3. The limits on N_A values are taken from published work on the number of cells in a given volume of cortex (*38*) and the range of percentage of myelinated axons in observed in a section of the macaque corpus callosum (*39*). The range of unmyelinated axonal radii in adult macaques (*39*) was used to bookend the range of initial nerve fiber radii, R_1. In Fig. 3E we plot the percentage of the increase of fiber radius, or $100*R_2/R_1$, which indicates the radial increase in myelination to account for the observed MTV change, as a percentage of the initial radius (x-axis) and number of axons (different curves).

Histological measurement of gray-level index (GLI)

In brief, the GLI measures the volume fraction of cell bodies in square fields of $20 \times 20 \mu m^2$ in cell body stained brain sections (20μm thick). GLI was calculated in cytoarchitectonic regions FG2 and FG3 in 10 postmortem brains. Full details of the definition of cytoarchitectonic regions FG2 and FG3 as well as the GLI are described in (*8, 9*). The GLI was calculated within ten equidistant bins spanning the cortical depth from 0% (layer I/II) to 100% (gray/white matter boundary) in three separate histological sections for each region in each hemisphere, and then averaged to obtain a mean GLI profile in each subject. The means of the 10

postmortem participants' GLI profiles of FG2 and FG3 were compared using a pairwise t-test. These data are presented in Fig. 3D.

Cortical curvature controls: Is development of T_1 related to changes in cortical curvature?

A remaining question is whether T_1 values may depend on curvature. First, it is possible that the development of T_1 may be due to development of curvature. Second, the differential T_1 across pFus-faces and CoS-places in adults may be due to differential curvature across gyri and sulci, as the latter is on a sulcus and the former is on a gyrus. To examine the effect of cortical curvature on T_1, we *(i)* examined if there is a general relationship between T1 and cortical curvature across adult cortex, *(ii)* determined if cortical curvature in pFus-faces changes with age, and *(iii)* estimated if there is a significant correlation between the mean cortical curvature and mean T_1 pFus-faces and CoS-places. Results indicate that curvature is not driving the development of T_1 for the following reasons:

(i) We do not find a consistent relationship between T_1 and curvature across macroanatomical structure such as gyri and sulci. While in adults, pFus-faces which is on a gyrus, has lower T_1 than CoS-places, which is on a sulcus, there is no general pattern across the cortex where sulci are generally associated with higher T_1 than gyri. This lack of a consistent relationship is shown in Fig. S7A-B. Fig S7A shows that the calcarine sulcus has a lower average T_1 than neighboring gryi. Fig. S7B shows that other sulci and gyri beyond primary sensory cortex, also show a reverse relationship with T_1 as compared to the CoS and the fusiform gyrus, e.g., the ascending branch of the inferior temporal sulcus and the superior temporal sulcus both demonstrate lower T_1 than surrounding gyri

(ii) We find no development of cortical curvature in VTC. Fig. S6C shows that cortical curvature does not change with age in right pFus-faces. Thus, curvature cannot explain developmental changes in T_1 observed in pFus-faces.

(iii) We find no correlation between curvature and T_1 across participants in either pFus-faces or CoS-places (Fig. S6E). Additionally, there is no correlation between the mean cortical curvature and T_1 across pFus-faces and CoS-places (Fig. S7D). Had cortical curvature been a determining factor in T_1 values, there should have been a significant relationship between T_1 and curvature.

Together these analyses indicate that development of T_1 is not due to curvature.

Cortical thickness controls: Is development of T_1 related to changes in cortical thickness?

One potential concern is that a misestimate of the *in vivo* gray/white matter boundary may affect T_1 measurements. We reasoned that if the observed T_1 changes in FG2 are due to increased myelination, which may erroneously label deep layers as white matter, FG2 would be thinner than FG3 in adults, but not children where we do not observe T_1 differences across FG2 and FG3. This effect would be potentially exacerbated if myelin content gradually changes between white and gray matter rather than exhibiting a sharp boundary between white and gray matter. These potential biases in estimating cortical thickness and their impact on T1 are schematized in Fig. S7I-L.

To address these issues, we conducted the following analyses: *(i)* We analyzed 6 unfixed, deeply frozen postmortem hemispheres that were cryo-sectioned and cell body as well as myelin stained in alternate histological sections. We then tested whether the gray/white boundary, and thus cortical thickness, is the same or different in cyto- and myeloarchitectonically defined conditions. *(ii)* We estimated cortical thickness of FG2 and FG3 from cell body stained sections in a sample of 10 postmortem paraffin fixed hemispheres and another sample of 6 unfixed, deeply frozen postmortem hemispheres that were cyro-sectioned. *(iii)* We estimated the cortical thickness of pFus-faces and CoS-places in our *in vivo* sample of 22 children and 24 adults using the tools in FreeSurfer. *(iv)* We correlated *in vivo* cortical thickness in CoS-places with mean T_1 across participants. *(v)* We assessed if cortical thickness can explain additional variance in functional selectivity in pFus-faces across participants through a multivariate linear model both using thickness and T_1 as predictors.

Results reveal that development of T_1 from childhood to adulthood as well as differential T_1 across pFus-faces and CoS-places in adults is likely not due to differences in cortical thickness:

(i) Figure S7B, D, F depicts an example of myelin stained section performed in 6 unfixed frozen and serially cryosectioned hemispheres. These examples show the sharp border between the cortical ribbon and the white matter in FG2, suggesting that there should be sufficient contrast to detect this boundary with MRI. Importantly, the boundary between white and gray matter revealed with the

myelin staining (Fig. S7B) coincides with this border (between layer VI and white matter) in alternating cell body stained sections (Fig. S7A). Finally, there were no acute differences in the pattern of myelination between FG2 and FG3, though a detailed study of the fine-grain myelination of FG2 and FG3 is beyond the scope of the present paper.

(ii) We measured the cortical thickness of FG2 and FG3 in two samples of postmortem brains. Sample 1 contained data from 10 formalin fixed, paraffin embedded postmortem hemispheres. Because of this histological processing the brain shrinks and therefore cortical thickness is corrected for linear shrinkage. This correction factor was calculated from the difference between the brain volume immediately after autopsy and the volume after histological processing, sectioning and 3D reconstruction. Sample 2 contained data of the 6 adult postmortmem hemispheres which were not fixed and not paraffin embedded to avoid shrinkage, but natively deep frozen. The observed thickness in our data are commensurate with prior measurements from Von. Economo and Koskinas (*40*), after correction for shrinkage. Contrary to the prediction that myelination of deep cortical layers would lead to thinner FG2 than FG3 in adults, measurements of cortical thickness in the postmortem brains reveal thicker FG2 than FG3 in the sample of unfixed, deeply frozen brains (Fig. S7G), and a similar but not significant difference in thickness in the fixed, paraffin embedded sample (Fig. S7G). These measurements in postmortem data suggest that differences in cortical thickness cannot account for our observation of differential T_1 between FG2 and FG3 in adults.

(iii) Measurements of cortical thickness in the *in vivo* samples are consistent with the measurements in the postmortem samples, and further show that in both adults and children pFus-faces (located in FG2) is thicker (not thinner as may be potentially caused by a higher myelin density in deeper cortical layers) than CoS-places, located in FG3 (Fig S7H).

(iv) Examination of the relationship between T_1 and cortical thickness shows that there is no significant correlation between T_1 and thickness across development in CoS-places (Fig. S8M). While there is a marginal correlation between T_1 and thickness

in right pFus-faces ($r = 0.32$, $p = 0.05$), there is no correlation between these factors after age was regressed out ($p = 0.87$), indicating that thickness and T_1 are independent factors and the apparent correlation was mediated by subject's age. Development of T_1 as well as differences across individuals are independent from cortical thickness.

(v) T_1 as a predictor of face selectivity explained 26% of the variance in functional selectivity for faces across participants in right pFus-faces (Fig. 2A). Adding cortical thickness as an additional predictor in the linear regression does not explain more variance and in fact slightly lowers model performance (25.7% variance explained). This suggests that face-selectivity in right pFus-faces is also not correlated with cortical thickness.

Together these analyses reveal that cortical thickness is not a parsimonious explanation of the differential T_1 development observed between pFus-faces and CoS-places.

Author contributions: JG: designed, collected, analyzed qMRI, fMRI, and behavioral data, and wrote the manuscript. MB: collected qMRI, fMRI and behavioral data, and analyzed qMRI data. VN: collected qMRI, fMRI, and behavioral data and analyzed fMRI data. AM: developed and optimized qMRI procedures. NPG: analyzed the postmortem histological stains regarding myelination, and cortical thickness. KSW, MB: analyzed the relation between functional and cytoarchitectonic ROIs. KA, KZ: collected and analyzed postmortem data regarding cell body density, myelination, cortical thickness, defined cytoarchitectonic ROIs, and contributed to the manuscript. KGS: designed and oversaw all components of the study, analyzed the relation between functional and cytoarchitectonic ROIs, and wrote the manuscript. All co-authors read and approved the submitted manuscript.

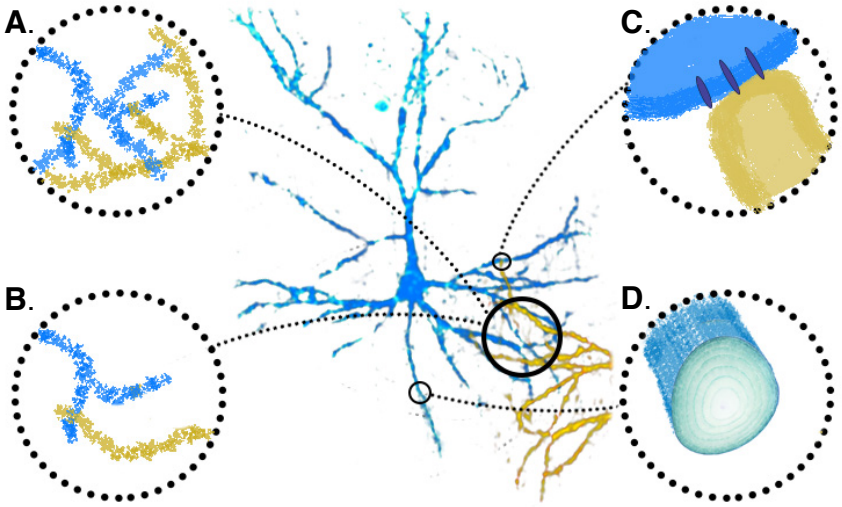

Fig. S1: Alternative models of developmental changes in tissue structure. Panels depict potential developmental changes of a cortical area's anatomical properties and their hypothesized effects on both macromolecular tissue volume (MTV) and T_1 (relaxation time). (**A**) Proliferation – dendritic arborizations interconnecting neighboring neurons complexify with development; This complexification can increase MTV, and decrease T_1. (**B**) Pruning – dendrites and axonal branches are slowly removed with time, leaving only essential connections. This would lead to decreases in MTV and increases in T_1. (**C**) Potentiation – Connections are strengthened at the synaptic and molecular level, such as receptor (dark ovals in dendrite membrane) exchange and upregulation. This mechanism should lead to no changes in either T_1 or MTV. (**D**) Projection – The myelination of axons increases. This would result in increased MTV and decreased T_1.

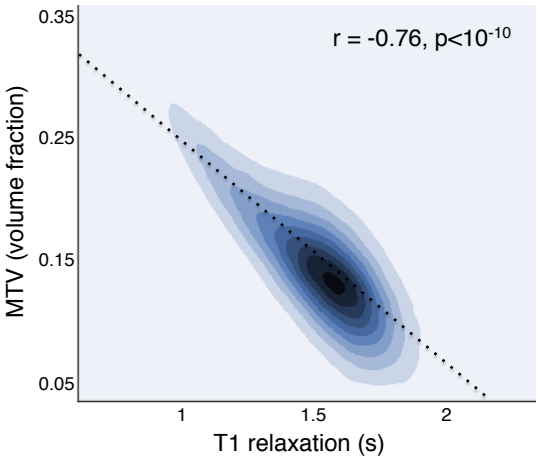

Fig. S2: Relationship between T_1 relaxation time (T_1) and macromolecular tissue volume (MTV). T_1 and MTV are plotted voxelwise, with voxels pooled bilaterally from the ventral temporal cortices of each subject. Value spread is summarized with a kernel density estimate, where darker shades correspond to higher density. Lower T_1 relaxation times are significantly correlated with higher macromolecular tissue volume.

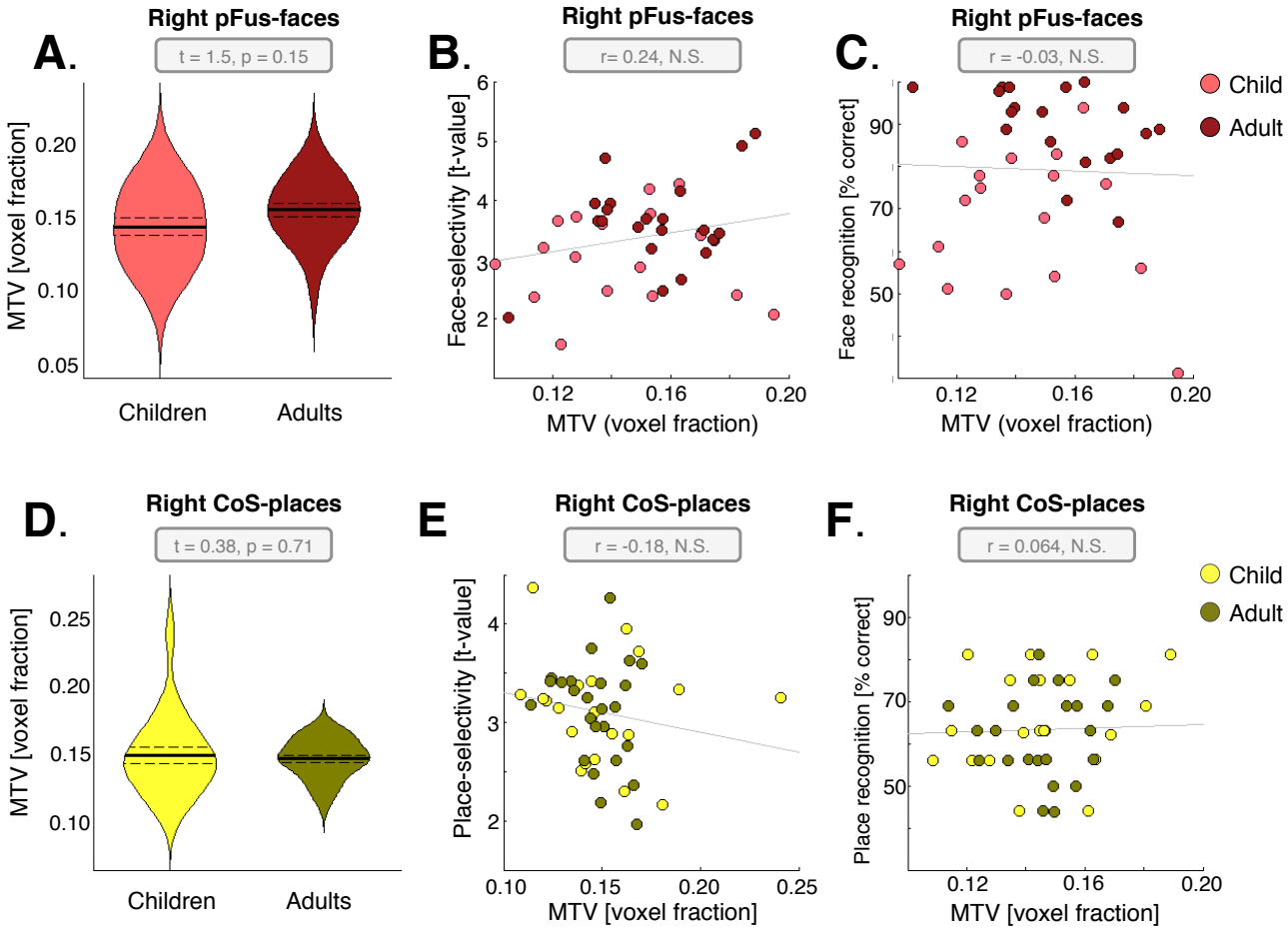

Fig. S3: Development of macromolecular tissue volume fraction (MTV) in pFus-faces and CoS-places and its relationship to function and behavior. (A) Mean MTV fraction in right pFus-faces in children (n=20, light red) and adults (n=20, dark red). **(B)** Mean face-selectivity (t-value) vs. MTV fraction. Dark colors are adults, light colors children. Each point is a participant. **(C)** Face recognition performance in the Cambridge Face Memory task (CFMT) vs. MTV fraction. **(D-F)** same as A-C but for right CoS-places. **(E)** Place-selectivity vs. MTV fraction. **(F)** Place recognition memory performance vs. MTV fraction; *pFus-faces* is also referred to as the fusiform face area one (FFA-1); *CoS-places* is also referred to as the parahippocampal place area (PPA).

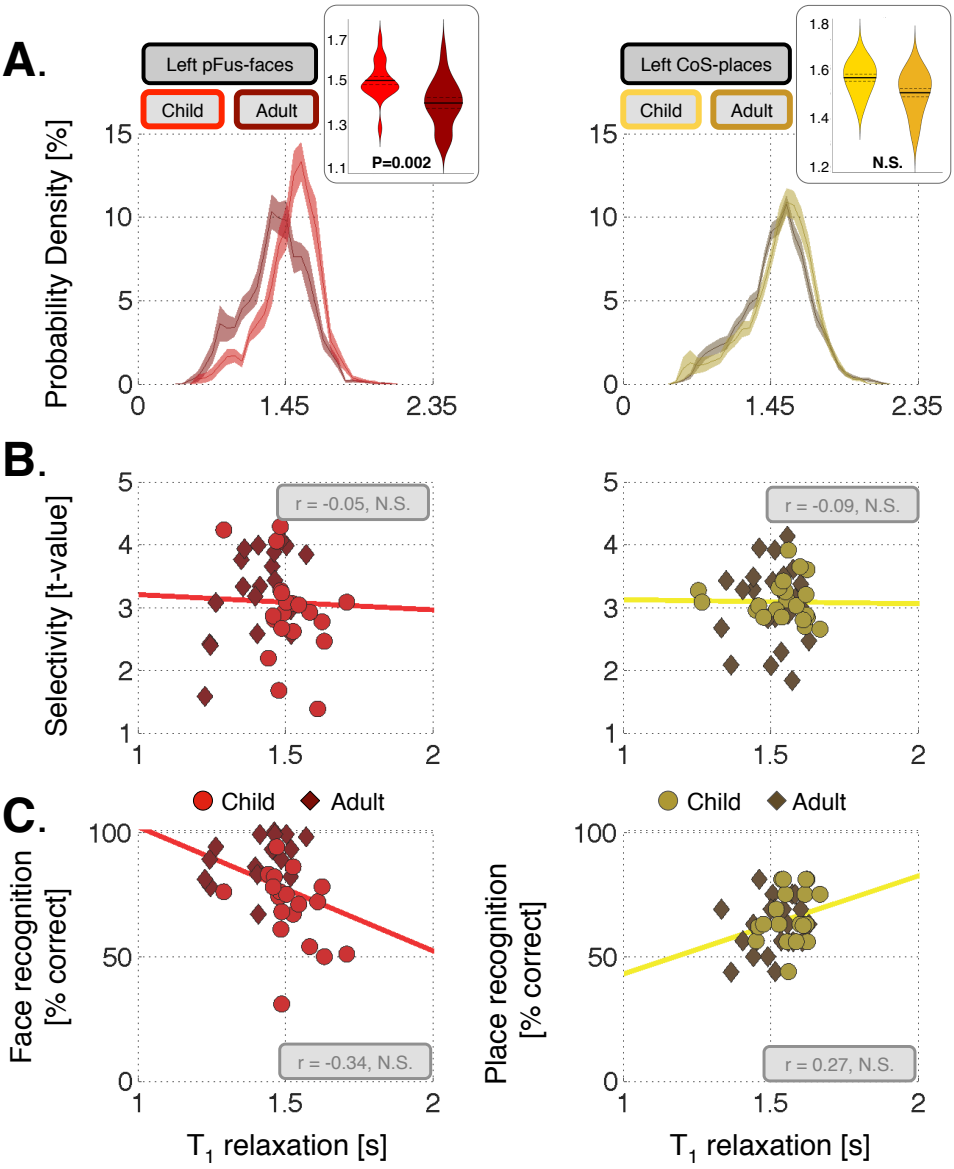

Fig. S4: Analyses of left hemisphere T_1 characteristics.
(A) Group and voxelwise distributions of T_1 in left pFus-faces and left CoS-places across children and adults. Similar to the right hemisphere, left pFus-faces shows a smaller but significant T_1 change from childhood (n=20) to adulthood (n=19). T_1 in left CoS-places, like the right hemisphere, shows no significant change from childhood (n=21) to adulthood (n=25). **(B)** While the data trend in the same direction as the right hemisphere, there is no significant relationship between selectivity for preferred stimulus category and T_1 in either place- or face-selective cortex in the left hemisphere. **(C)** No significant correlations between recognition memory accuracy and T_1 in left pFus-faces and CoS-places. The CFMT vs. T_1 correlations across right and left pFus-faces are not significantly different. In (B,C) Each point represents a participant. *Diamonds:* adults; *Circles:* children.

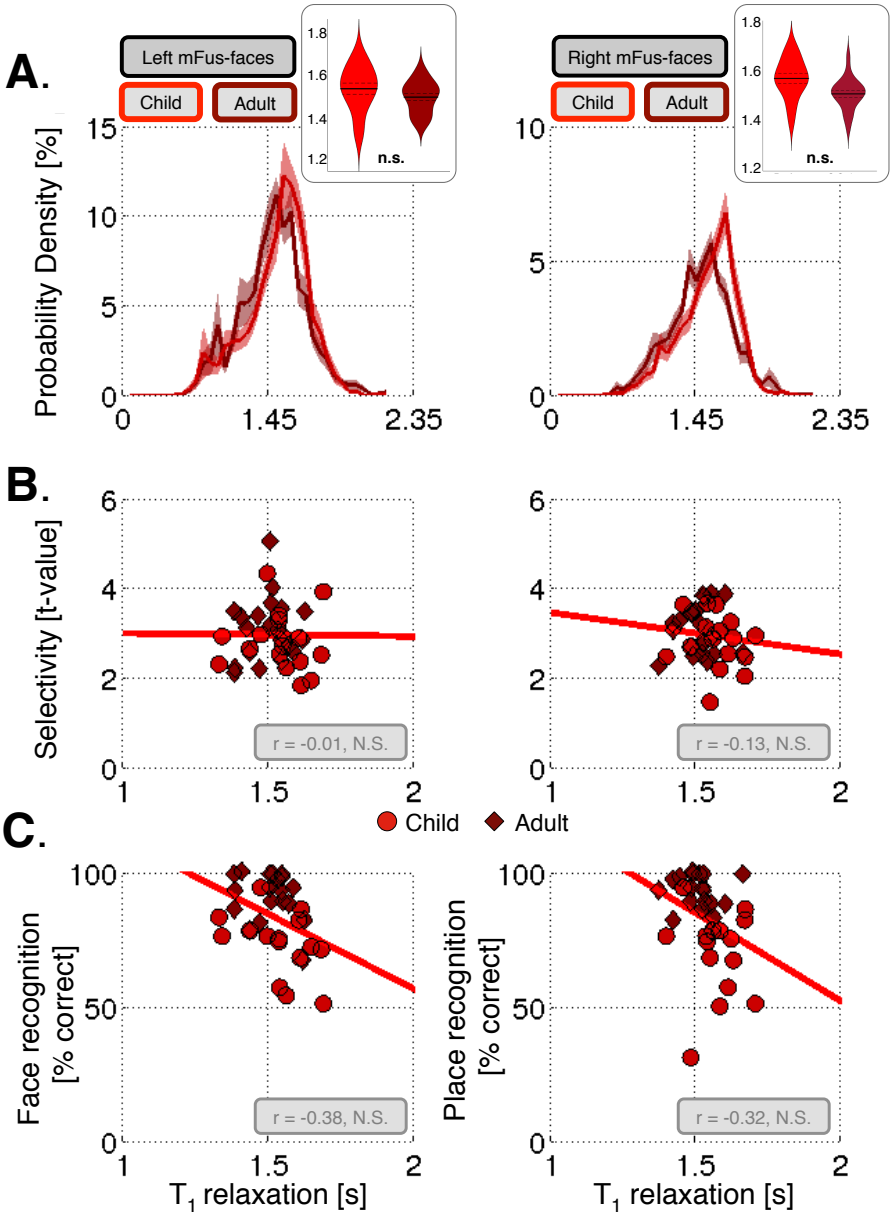

Fig. S5: T_1 properties of mFus-faces across development.
(A) Group and voxelwise distributions of T_1 in left mFus-faces (16 children, 21 adults) and right mFus-faces (16 children, 21 adults). T_1 values from mFus-faces in the right and left hemispheres are plotted in light red for children and dark red for adults. In the upper inset, the average T_1 in mFus-faces is compared between adults and children. Violin plot thickness illustrates the density of participants, solid black lines show group mean, and dotted black lines are standard error; *n.s.*: not significant. Lower histograms illustrate the average distribution of T_1 across voxels within mFus-faces across participants (shaded region is standard error). **(B)** No significant correlations between T_1 and selectivity for faces in left and right mFus-faces. Each point is a participant. *Diamonds:* adults; *Circles:* children. Mean T_1 from each participant's fROI is plotted against its selectivity for faces; *n.s.*: not significant. **(C)** Correlations between face recognition memory accuracy and T_1 in left and right mFus-faces. Performance on the Cambridge face memory test (CFMT) shows a trend for a negative (but not significant) correlation T_1 values in mFus-faces. The CFMT vs. T_1 correlations across right pFus- and mFus-faces are not significantly different. *Diamonds:* adults; *Circles:* children; Each point represents a participant; mFus-faces is also referred to as fusiform face area two (FFA-2).

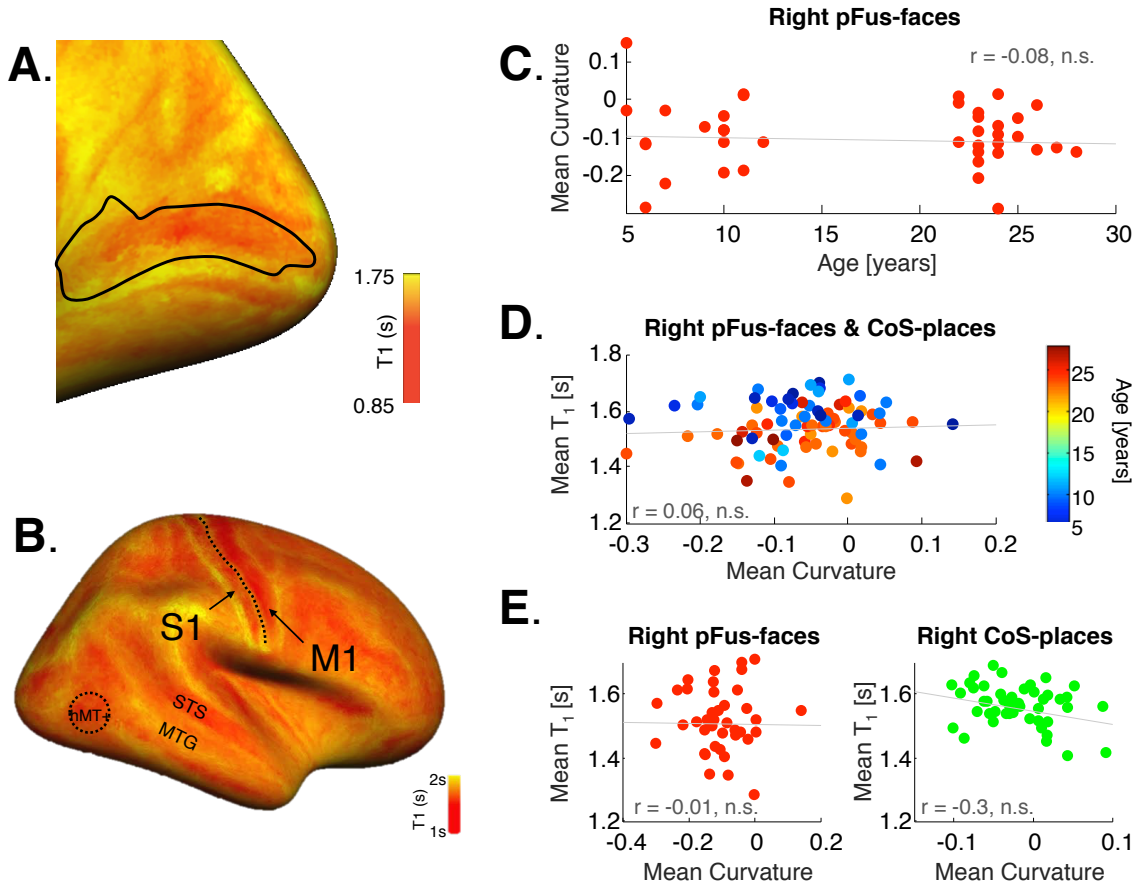

Fig. S6: The relationship between cortical curvature and T_1. Panels show the average of 20 adults' T_1 maps that were registered using cortex-based alignment to the FreeSurfer average brain surface. **(A)** Zoomed view of average T_1 map around the calcarine sulcus (indicated in the black outline). The pericalcarine ROI has been delineated in black, the center of which is the fundus of the calcarine sulcus. Color indicates the average T_1 in seconds in each point (see colorbar). Calcarine sulcus occupies a region of low T_1 relaxation time and surrounding gyri have a higher T_1. **(B)** Several additional examples where sulci have lower T_1 than gyri. Average T_1 map on the lateral view of the FreeSurfer average brain surface. Somatosensory cortex (S1) posterior to the central sulcus (fundus of the sulcus is traced with dotted line) and motor cortex (M1) anterior to the central sulcus, along with the human MT complex (hMT+) in the posterior inferior temporal sulcus are highly myelinated regions, consequently showing low T_1. In the superior temporal lobe, the superior temporal sulcus (STS) shows lower T_1 than the adjacent middle temporal gyrus. **(C)** The average cortical curvature from right pFus-faces, assessed using FreeSurfer, does not change with age. The developmental change in T_1 in pFus-faces is thus not a result of curvature. **(D)** Mean cortical curvature in right pFus-faces and CoS-places is not related to mean T_1. Each participant is associated with two points, one point depicting the mean curvature and T_1 for CoS-places, and the other for pFus-faces. Participants are colored by age. In this dataset, curvature can thus not explain differences in T1 between regions. **(E)** Even within individual fROIs, there is no significant correlation between corticl curvature and T_1.

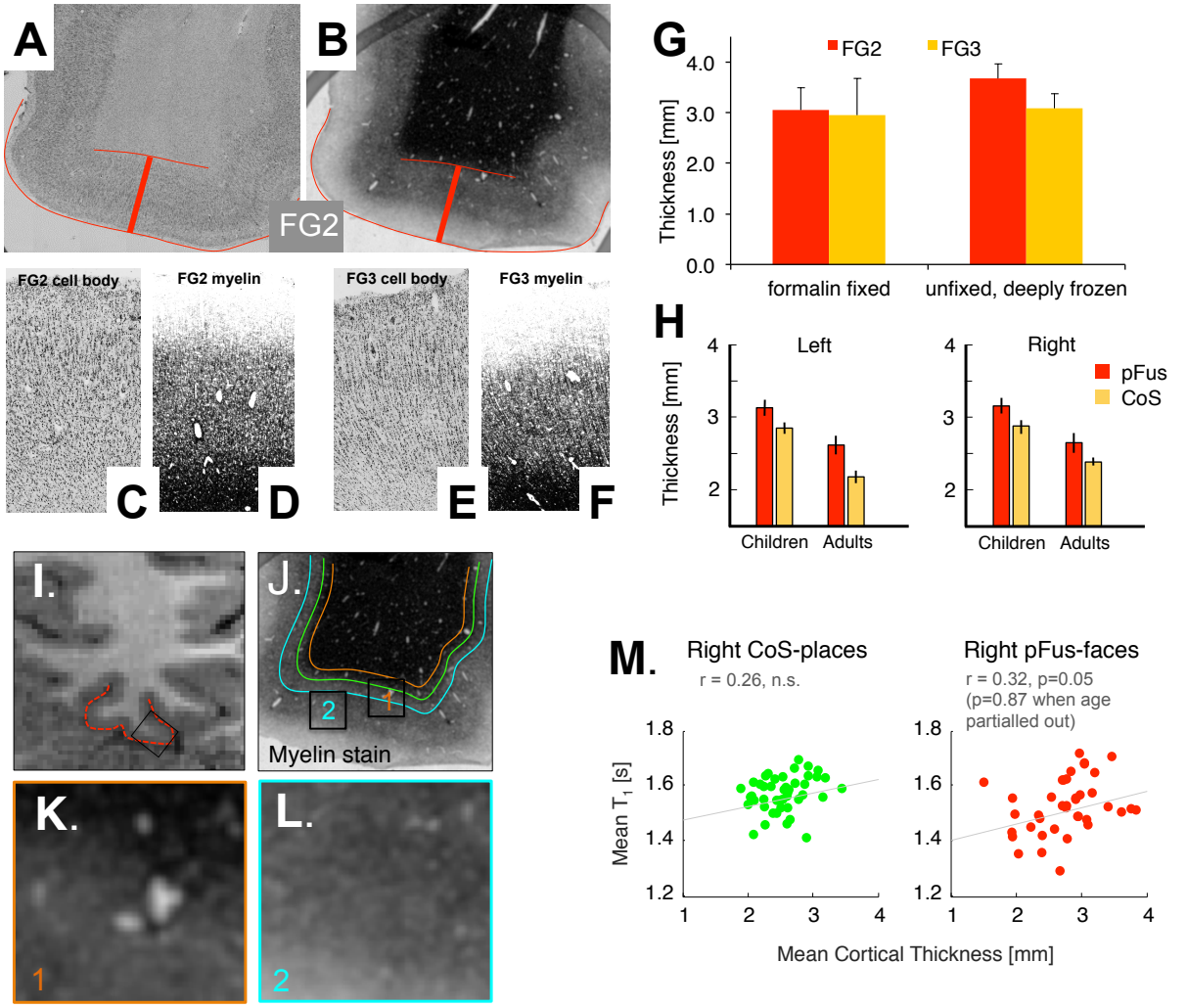

Fig. S7: *Ex vivo* and *in vivo* examinations of cortical thickness, myelination, and the relationship to T_1. Cell body stained **(A, C, E)** and myelin stained **(B, D, F)** sections through fusiform areas FG2 **(A-D)** and FG3 **(E-F),** and their cortical thickness **(G)** compared to *in vivo* measurements **(H)**. In **(A,C,E)** darker colors indicate cell bodies. In **(B,D,F)** darker colors illustrate higher myelin content. The bold red line in (A) and (B) indicates the thickness of the cortex in FG2, which is identical in the cell body and myelin stains of adjacent sections. The thin red lines indicate the pial surface and the cortex/white matter border, respectively. A clear contrast is visible between the myelin density in the cortical ribbon and the higher density in the white matter. The myelin stained sections therefore demonstrate a gray/white matter border in FG2 and FG3 that coincides with the border between layer VIb and the white matter in cytoarchitectonic studies. In **(C-F)** the deeper layers are at the bottom of the image and the superficial layers are at the top. **(D)** and **(F)** demonstrate a comparable myelin density in areas FG2 and FG3. This pattern of results shown in panels **(A-F)** was observed in six unfixed frozen and serially cryosectioned hemispheres. **(G)** shows the cortical thickness measured in histological sections (20 µm section thickness) of a sample of 10 formalin fixed and paraffin embedded (shrinkage corrected) hemispheres and in a sample of 6 unfixed, deep frozen hemispheres. In both samples, but particularly in the unfixed, deeply frozen sample, the thickness of FG2 is higher than in FG3. **(H)** Cortical thickness measured in the *in vivo* participants shows thicker cortex in pFus-faces than in CoS-places, in both children (n=22) and adults (n=23). This difference in thickness between pFus and CoS remains identical despite cortical thinning during development. Main effect of age ($F(1,147) = 60.4$, $p<0.001$), main effect of fROI ($F(1,147) = 20.3$, $p<0.001$), no significant interaction ($F(1,147) = 0.28$, n.s). **(I)** The fusiform gyrus (FG), outlined in red dashed line. The gyral crown, outlined in a black square, is an example of the location of the myelin-stained section magnified in the next panel (not the same subject). **(J)** Myelin stain section of the FG. Darker pixels have more myelin content. The true gray-white boundary is outlined in green. Orange border delineates a cortical boundary that may result in individuals in which myelination has not yet completed (e.g. children). Less myelin would make voxels at the cortical boundary appear darker in anatomical MRI images resulting an overestimation of cortical thickness. The cyan outline denotes a cortical boundary that may result in individuals in which axons have been heavily myelinated (e.g. adults), biasing the deeper cortical layers towards being labeled as white matter, consequently, underestimating the cortical thickness. Black squares numbered 1 and 2 are voxels near the cortical boundary defined in either the thickness overestimate or underestimate cases. **(K)** A voxel at the cortical boundary in cortex that has been overestimated in thickness. This voxel would contain more white matter than typical gray voxels, consequently lowering T_1 relaxation time. As children have thicker cortex than adults, this type of bias would be larger in children and would predict lower T_1 in children‘s gray matter than adults‘ due to higher myelin content. However, this is opposite to our observations of higher T_1 in children’s fusiform gyrus. **(L)** A voxel at the cortical boundary in the case in which thickness has been underestimated. This voxel samples more superficial layers of cortex, which are lightly myelinated and lightly populated with cells, resulting in higher T_1 relaxation times. As underestimating cortical thickness is a potential bias in adults who have thinner cortex, this bias would lead to higher T_1 in adults than children, which is again opposite to our observations in the FG. **(M)** T_1 was not correlated with thickness within CoS-places. There was a marginal correlation between T_1 and thickness in right pFus-faces ($r = 0.32$, $p = 0.05$), but this correlation was not significant after age was regressed out ($p = 0.87$), indicating that thickness and T_1 are independent.

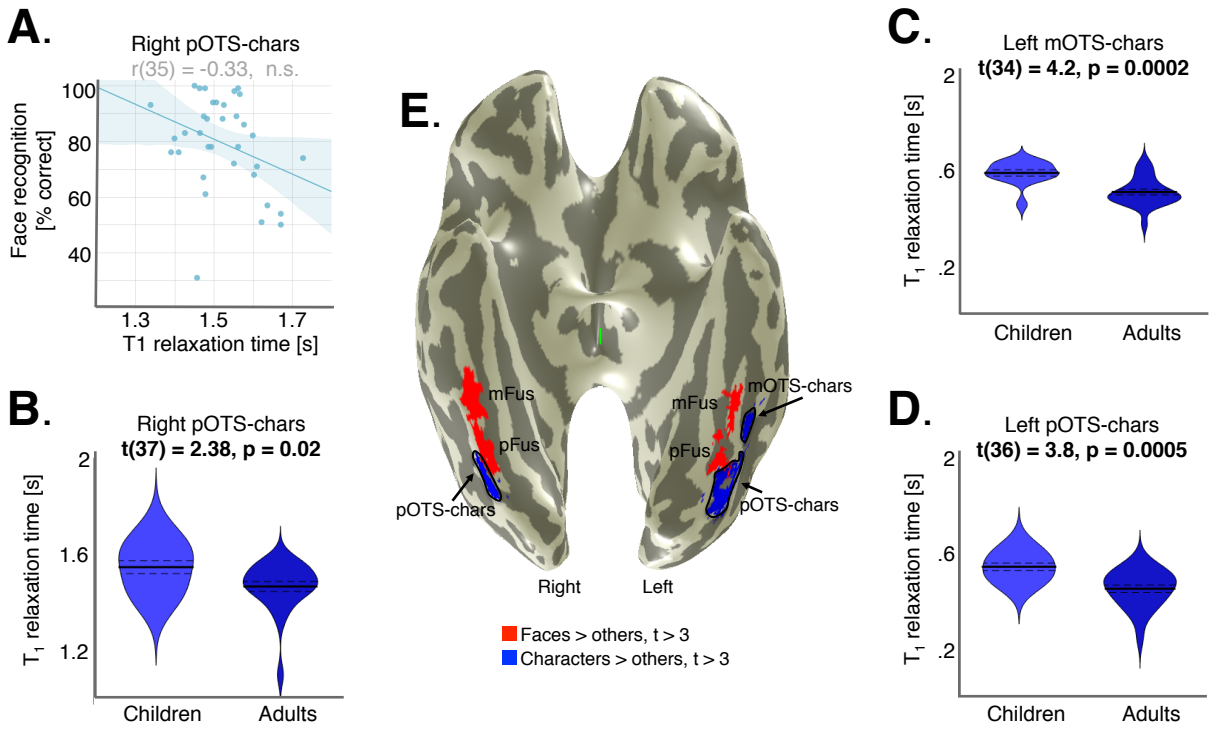

Fig. S8: Development of T_1 relaxation time in character-selective cortex. (A) T_1 in right pOTS1-chars abutting the pFus face-selective region does not correlate with performance in the Cambridge Face Recognition Memory Task (CFMT). Removing floor and ceiling performance subjects (>98%, <33%) and regressing out the variable of age, this correlation remains non-significant. This suggests a tight spatial correspondence between tissue development and behavior. The correlation between CFMT and T_1 in left pOTS-chars (r(34)=-.36, n.s.) or mOTS-chars (r(33)=-.57, n.s.) were also not significant. **(B)** T_1 in right pOTS-chars in children (n=15, light blue) is significantly longer than adults (n=24, dark blue). **(C)** T_1 in left mOTS-chars in children (n=13) is significantly longer than adults (n=23). **(D)** T_1 in left pOTS-chars in children (n=13) is significantly longer than adults (n=25). **(E)** Face-selective (red) and character-selective (blue) regions highlighted on an example six year old female, rendered on an inflated cortical surface of the ventral temporal lobes. Character selective regions (pseudowords, numbers > faces, bodies, scenes, objects, t>3, voxel level) are located on the posterior occipitotemporal sulcus (pOTS-chars) bilaterally, and on the middle occipitotemporal sulcus (mOTS-chars) in the left hemisphere. Not all fROIs were found in all subjects (see Table S1 for details); *pOTS-chars* is also referred to as the visual word form area 1 (VWFA1); *mOTS-chars* is also referred to as the visual word form area 2 (VWFA2).

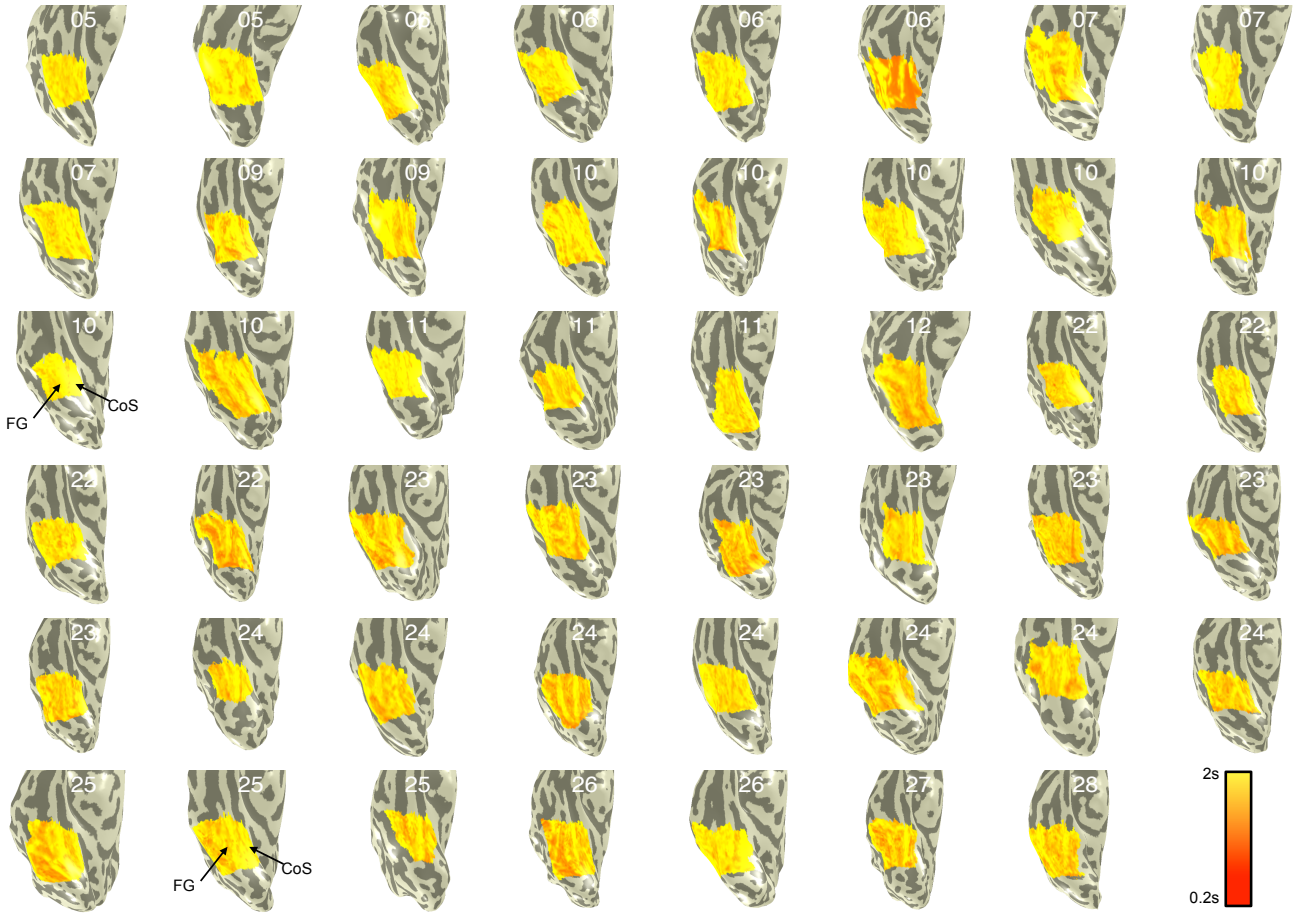

Fig. S9: T_1 relaxation time within ventral temporal cortex (VTC) shown on the right hemisphere ventral view of the inflated cortical surface in each subject. Brains are arranged in ascending age; the age of each subject is displayed in the upper right corner of each cortical surface. T_1 maps are presented within an anatomically defined VTC mask. The VTC mask is defined laterally by the inferior temporal gyrus, posteriorly by the posterior transverse collateral sulcus, medially by the parahippocampal gyrus, and anteriorly with a plane drawn at the posterior-most extent of the hippocampus. In general, in adults but not children, T_1 relaxation time is lower in the fusiform gyrus, than the collateral suclus. FG: Fusiform Gyrus; CoS: Collateral Sulcus.

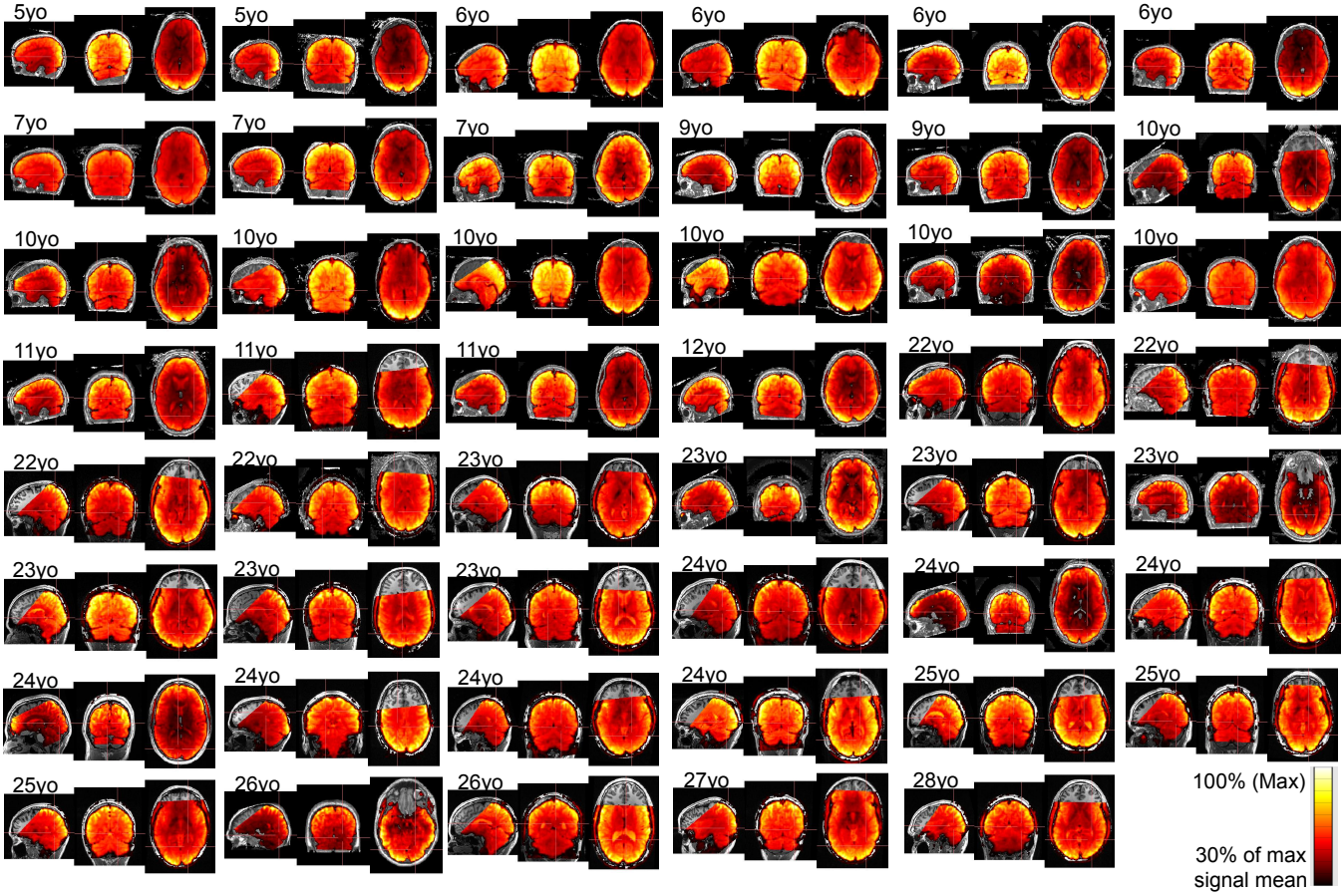

Fig. S10: Functional maps are well-aligned to quantitative anatomical images in each subject. The mean signal was calculated in each subject as the mean of all functional runs (arbitrary scanner units). The mean map was thresholded in each subject to a value near 30% of the maximum mean signal to better visualize the functional envelope of the brain and its alignment to the underlying anatomy. Age of each subject is labeled above each brain.

References and Notes

1. G. Golarai, D. G. Ghahremani, S. Whitfield-Gabrieli, A. Reiss, J. L. Eberhardt, J. D. Gabrieli, K. Grill-Spector, Differential development of high-level visual cortex correlates with category-specific recognition memory. *Nat. Neurosci.* **10**, 512–522 (2007). Medline

2. K. S. Scherf, M. Behrmann, K. Humphreys, B. Luna, Visual category-selectivity for faces, places and objects emerges along different developmental trajectories. *Dev. Sci.* **10**, F15–F30 (2007). doi:10.1111/j.1467-7687.2007.00595.x Medline

3. J. F. Cantlon, P. Pinel, S. Dehaene, K. A. Pelphrey, Cortical representations of symbols, objects, and faces are pruned back during early childhood. *Cereb. Cortex* **21**, 191–199 (2011). doi:10.1093/cercor/bhq078 Medline

4. A. Mezer, J. D. Yeatman, N. Stikov, K. N. Kay, N.-J. Cho, R. F. Dougherty, M. L. Perry, J. Parvizi, H. Hua, K. Butts-Pauly, B. A. Wandell, Quantifying the local tissue volume and composition in individual brains with magnetic resonance imaging. *Nat. Med.* **19**, 1667–1672 (2013). doi:10.1038/nm.3390 Medline

5. A. Lutti, F. Dick, M. I. Sereno, N. Weiskopf, Using high-resolution quantitative mapping of R1 as an index of cortical myelination. *Neuroimage* **93**, 176–188 (2014). doi:10.1016/j.neuroimage.2013.06.005 Medline

6. P. Rakic, J. P. Bourgeois, M. F. Eckenhoff, N. Zecevic, P. S. Goldman-Rakic, Concurrent overproduction of synapses in diverse regions of the primate cerebral cortex. *Science* **232**, 232–235 (1986). doi:10.1126/science.3952506 Medline

7. G. N. Elston, I. Fujita, Pyramidal cell development: Postnatal spinogenesis, dendritic growth, axon growth, and electrophysiology. *Front. Neuroanat.* **8**, 78 (2014). doi:10.3389/fnana.2014.00078 Medline

8. J. Caspers, K. Zilles, S. B. Eickhoff, A. Schleicher, H. Mohlberg, K. Amunts, Cytoarchitectonical analysis and probabilistic mapping of two extrastriate areas of the human posterior fusiform gyrus. *Brain Struct. Funct.* **218**, 511–526 (2013). Medline

9. S. Lorenz, K. S. Weiner, J. Caspers, H. Mohlberg, A. Schleicher, S. Bludau, S. B. Eickhoff, K. Grill-Spector, K. Zilles, K. Amunts, Two new cytoarchitectonic areas on the human mid-fusiform gyrus. *Cereb. Cortex.* 1–13 (2015). doi:10.1093/cercor/bhv225 Medline

10. K. S. Weiner, M. A. Barnett, S. Lorenz, J. Caspers, A. Stigliani, K. Amunts, K. Zilles, B. Fischl, K. Grill-Spector, The cytoarchitecture of domain-specific regions in human high-level visual cortex. *Cereb. Cortex* 10.1093/cercor/bhw361 (2016). doi:10.1093/cercor/bhw361 Medline

11. B. Fischl, M. I. Sereno, A. M. Dale, Cortical surface-based analysis. II: Inflation, flattening, and a surface-based coordinate system. *Neuroimage* **9**, 195–207 (1999). doi:10.1006/nimg.1998.0396 Medline

12. S. R. Olsen, R. I. Wilson, Lateral presynaptic inhibition mediates gain control in an olfactory circuit. *Nature* **452**, 956–960 (2008). doi:10.1038/nature06864 Medline

13. S. Ryglewski, D. Kadas, K. Hutchinson, N. Schuetzler, F. Vonhoff, C. Duch, Dendrites are dispensable for basic motoneuron function but essential for fine tuning of behavior. *Proc. Natl. Acad. Sci. U.S.A.* **111**, 18049–18054 (2014). doi:10.1073/pnas.1416247111 Medline

14. D. E. Wilson, D. E. Whitney, B. Scholl, D. Fitzpatrick, Orientation selectivity and the functional clustering of synaptic inputs in primary visual cortex. *Nat. Neurosci.* **19**, 1003–1009 (2016). doi:10.1038/nn.4323 Medline

15. J. D. Yeatman, B. A. Wandell, A. A. Mezer, Lifespan maturation and degeneration of human brain white matter. *Nat. Commun.* **5**, 4932 (2014). doi:10.1038/ncomms5932 Medline

16. C. Lebel, C. Beaulieu, Longitudinal development of human brain wiring continues from childhood into adulthood. *J. Neurosci.* **31**, 10937–10947 (2011). doi:10.1523/JNEUROSCI.5302-10.2011 Medline

17. N. Baumann, D. Pham-Dinh, Biology of oligodendrocyte and myelin in the mammalian central nervous system. *Physiol. Rev.* **81**, 871–927 (2001). Medline

18. B. A. Barres, M. C. Raff, Proliferation of oligodendrocyte precursor cells depends on electrical activity in axons. *Nature* **361**, 258–260 (1993). doi:10.1038/361258a0 Medline

19. C. Stüber, M. Morawski, A. Schäfer, C. Labadie, M. Wähnert, C. Leuze, M. Streicher, N. Barapatre, K. Reimann, S. Geyer, D. Spemann, R. Turner, Myelin and iron concentration in the human brain: A quantitative study of MRI contrast. *Neuroimage* **93**, 95–106 (2014). doi:10.1016/j.neuroimage.2014.02.026 Medline

20. Y. Sagi, I. Tavor, S. Hofstetter, S. Tzur-Moryosef, T. Blumenfeld-Katzir, Y. Assaf, Learning in the fast lane: New insights into neuroplasticity. *Neuron* **73**, 1195–1203 (2012). doi:10.1016/j.neuron.2012.01.025 Medline

21. M. V. Peelen, B. Glaser, P. Vuilleumier, S. Eliez, Differential development of selectivity for faces and bodies in the fusiform gyrus. *Dev. Sci.* **12**, F16–F25 (2009). doi:10.1111/j.1467-7687.2009.00916.x Medline

22. G. Golarai, A. Liberman, K. Grill-Spector, Experience shapes the development of neural substrates of face processing in human ventral temporal cortex. *Cereb. Cortex* bhv314 (2015). doi:10.1093/cercor/bhv314 Medline

23. K. Grill-Spector, G. Golarai, J. Gabrieli, Developmental neuroimaging of the human ventral visual cortex. T*rends Cogn. Sci.* **12**, 152–162 (2008). doi:10.1016/j.tics.2008.01.009 Medline

24. G. Golarai, A. Liberman, J. M. Yoon, K. Grill-Spector, Differential development of the ventral visual cortex extends through adolescence. *Front. Hum. Neurosci.* **3**, 80 (2010). Medline

25. W. D. Rooney, G. Johnson, X. Li, E. R. Cohen, S.-G. Kim, K. Ugurbil, C. S. Springer Jr., Magnetic field and tissue dependencies of human brain longitudinal $^{1}H_2O$ relaxation in vivo. *Magn. Reson. Med.* **57**, 308–318 (2007). doi:10.1002/mrm.21122 Medline

26. A. Mezer, A. Rokem, S. Berman, T. Hastie, B. A. Wandell, Evaluating quantitative proton-density-mapping methods. *Hum. Brain Mapp.* **37**, 3623–3635 (2016). doi:10.1002/hbm.23264 Medline

27. D. A. Feinberg, K. Setsompop, Ultra-fast MRI of the human brain with simultaneous multi-slice imaging. *J. Magn. Reson.* **229**, 90–100 (2013). doi:10.1016/j.jmr.2013.02.002 Medline

28. A. Stigliani, K. S. Weiner, K. Grill-Spector, Temporal Processing Capacity in High-Level Visual Cortex Is Domain Specific. *J. Neurosci.* **35**, 12412–12424 (2015). doi:10.1523/JNEUROSCI.4822-14.2015 Medline

29. N. Kanwisher, J. McDermott, M. M. Chun, The fusiform face area: A module in human extrastriate cortex specialized for face perception. *J. Neurosci.* **17**, 4302–4311 (1997). Medline

30. R. Epstein, N. Kanwisher, A cortical representation of the local visual environment. *Nature* **392**, 598–601 (1998). doi:10.1038/33402 Medline

31. S. Dehaene, G. Le Clec'H, J. B. Poline, D. Le Bihan, L. Cohen, The visual word form area: A prelexical representation of visual words in the fusiform gyrus. *Neuroreport* **13**, 321–325 (2002). doi:10.1097/00001756-200203040-00015 Medline

32. M. Ben-Shachar, R. F. Dougherty, G. K. Deutsch, B. A. Wandell, Differential sensitivity to words and shapes in ventral occipito-temporal cortex. *Cereb. Cortex* **17**, 1604–1611 (2007). doi:10.1093/cercor/bhl071 Medline

33. S. Carey, R. Diamond, B. Woods, Development of Face Recognition - A Maturational Component? *Dev. Psychol.* **16**, 257–269 (1980). doi:10.1037/0012-1649.16.4.257

34. S. Weigelt, K. Koldewyn, D. D. Dilks, B. Balas, E. McKone, N. Kanwisher, Domain-specific development of face memory but not face perception. *Dev. Sci.* **17**, 47–58 (2014). doi:10.1111/desc.12089 Medline

35. L. T. Germine, B. Duchaine, K. Nakayama, Where cognitive development and aging meet: Face learning ability peaks after age 30. *Cognition* **118**, 201–210 (2011). doi:10.1016/j.cognition.2010.11.002 Medline

36. K. A. Dalrymple, L. Garrido, B. Duchaine, Dissociation between face perception and face memory in adults, but not children, with developmental prosopagnosia. *Dev. Cogn. Neurosci.* **10**, 10–20 (2014). doi:10.1016/j.dcn.2014.07.003 Medline

37. B. Duchaine, K. Nakayama, The Cambridge Face Memory Test: Results for neurologically intact individuals and an investigation of its validity using inverted face stimuli and prosopagnosic participants. *Neuropsychologia* **44**, 576–585 (2006). doi:10.1016/j.neuropsychologia.2005.07.001 Medline

38. C. N. Carlo, C. F. Stevens, Structural uniformity of neocortex, revisited. *Proc. Natl. Acad. Sci. U.S.A.* **110**, 1488–1493 (2013). doi:10.1073/pnas.1221398110 Medline

39. A. S. Lamantia, P. Rakic, Cytological and quantitative characteristics of four cerebral commissures in the rhesus monkey. *J. Comp. Neurol.* **291**, 520–537 (1990). doi:10.1002/cne.902910404 Medline

40. C. von Economo, G. N. Koskinas, *The Cytoarchitectonics of the Adult Human Cortex* (Julius Springer Verlag, 1925).